

Non-Hermitian Boundary Modes and Topology

Dan S. Borgnia, Alex Jura Kruchkov, and Robert-Jan Slager

Department of Physics, Harvard University, Cambridge, Massachusetts 02138, USA

 (Received 3 May 2019; revised manuscript received 25 November 2019; accepted 17 January 2020; published 7 February 2020)

We consider conditions for the existence of boundary modes in non-Hermitian systems with edges of arbitrary codimension. Through a universal formulation of formation criteria for boundary modes in terms of local Green's functions, we outline a generic perspective on the appearance of such modes and generate corresponding dispersion relations. In the process, we explain the skin effect in both topological and nontopological systems, exhaustively generalizing bulk-boundary correspondence to different types of non-Hermitian gap conditions, a prominent distinguishing feature of such systems. Indeed, we expose a direct relation between the presence of a point gap invariant and the appearance of skin modes when this gap is trivialized by an edge. This correspondence is established via a doubled Green's function, inspired by doubled Hamiltonian methods used to classify Floquet and, more recently, non-Hermitian topological phases. Our work constitutes a general tool, as well as a unifying perspective for this rapidly evolving field. Indeed, as a concrete application we find that our method can expose novel non-Hermitian topological regimes beyond the reach of previous methods.

DOI: [10.1103/PhysRevLett.124.056802](https://doi.org/10.1103/PhysRevLett.124.056802)

The absence of Hermiticity allows new symmetries and promises novel topological phases [1–8]. Recent experiments [9–13] observe generalizations of concepts from Hermitian systems [5,8], but depend on fine-tuned gain and loss symmetries, e.g., \mathcal{PT} symmetry [10]. Some aspects appear counterintuitive, such as the pileup of bulk states at system edges, the non-Hermitian skin effect [6,14–16], which suggests an absence of bulk-boundary correspondences [5,14,17,18]—boundary modes reflecting topological degeneracy in the bulk spectrum [19–26] that lay the foundation for the classification and observation of topological phases [27,28].

We introduce a general framework, resting on universal Green's function classification methods [27], to formulate an exhaustive description of boundary modes and their connection to bulk topology. Through this physical observable, we generalize notions of bulk-boundary correspondence, explain non-Hermitian skin effects, and uncover novel topological regimes. Particularly, an otherwise Hermitian system is tuned from one nontrivial topological phase to another by adding generic non-Hermiticity, suggesting unexplored, experimentally accessible, properties of systems under open conditions.

Non-Hermitian band topology.—While Hermitian symmetry protected topological phases (SPTs) are classified with respect to a real band gap [19–26], non-Hermitian systems have complex spectra. Accordingly, there are band gaps and point gaps, marked orange in Fig. 1. Band gaps are either a line gap [Fig. 1(a)] or the closed region between two bands [Fig. 1(c)]. They generate two disjoint simply connected regions of the complex plane just as a Hermitian band gap. Point gaps are the region enclosed by a *single*

band in the complex plane, Fig. 1(b) [1,3]. Topology is defined with respect to a band center [stars in Figs. 1(b) and 1(c)], generating a simply connected punctured plane, whose topology is different from that of two disjoint regions. A point gap invariant can be visualized as a net system vorticity [5]. This geometric interpretation will guide the development of our formalism below. In fact, it implies bulk topological invariants must change as line gaps close into point gaps through crossings of isolated bands [Fig. 1(b)] [1,3,5]. This is visualized by unwrapping the punctured complex plane into an open strip (Fig. 1) via a holomorphic map, detailed in the Supplemental Material I [29].

Diagnosing edge-localized bound states.—All formation criteria for edge modes can be obtained from in-gap zeros of the Green's function projected to relevant edges [27,28]. The idea is that the Green's function of a system with an on-site potential \mathcal{V} is given by

$$G(\omega, \mathbf{k}) = [1 - G_0(\omega, \mathbf{k})\mathcal{V}]^{-1}G_0(\omega, \mathbf{k}), \quad (1)$$

where indices on the possible matrix structure for \mathcal{V} are suppressed and G_0 is the impurity free Green's function. Projecting to an edge, poles correspond to

$$\det[G_0(\omega, \mathbf{k}_{\parallel}, \mathbf{r}_{\perp} = 0)\mathcal{V} - \mathbf{1}] = 0, \quad (2)$$

where \mathbf{k}_{\parallel} and \mathbf{r}_{\perp} refer to the momenta and perpendicular coordinates along edges of arbitrary codimension [27].

By virtue of bulk-boundary correspondence, Hermitian topological phases must have in-gap solutions of Eq. (2) for any impurity strength approaching an edge, $|\mathcal{V}| \rightarrow \infty$ [27]. Therefore, zeros of the restricted in-gap Green's function,

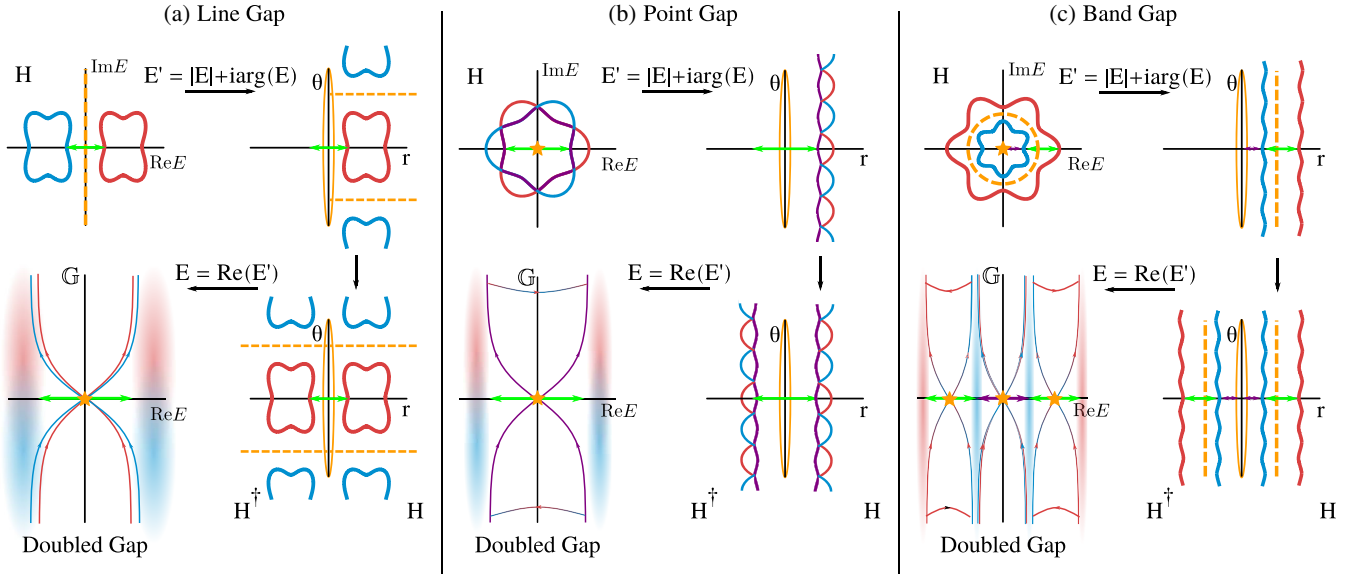


FIG. 1. Non-Hermitian gap topology. Top rows illustrate the holomorphic mapping of non-Hermitian bands (see Supplemental Material [29]) on the punctured complex plane ($\mathcal{C} - \{0\}$) to a strip, parametrized (r, θ) (green/purple arrows indicate gaps). Systems are then duplicated along the right column of each panel, $\hat{H}^\dagger \rightarrow -r$ and $\hat{H} \rightarrow +r$, where we note that generically the shape is altered. Bands are collapsed to real line in bottom rows, and we plot in-gap doubled Green's functions across different band gaps (orange markers) with blue-red smears representing Bloch bands. Curves crossing the gap depict the topological example (Fig. 2) of in-gap doubled Green's function \mathbb{G} eigenvalues, see Eq. (4). A line gap (a) protects zeros of \mathbb{G} crossing from red (blue) to blue (red) bands, while bands in (c) may have both point gap invariants (crossing zero in purple gap) and band gap invariants (red to blue).

$G_0(\epsilon, \mathbf{k}_\parallel, \mathbf{r}_\perp = 0)$, correspond to topological edge-localized states, see Supplemental Material [29], Secs. II and III. And, locations of the Green's function zeros $\omega_*(\mathbf{k}_\parallel)$ define dispersion relations of edge modes. Furthermore, counting Green's function zeros between bands determines band topological invariants [60], see Supplemental Material III [29].

Doubled Green's function.—We cannot directly apply the above formalism to a non-Hermitian system, \hat{H}_0 ; see Supplemental Material III [29]. We, therefore, define a Hermitian doubled Hamiltonian [1,3,61],

$$\hat{\mathbb{H}}_0 = \begin{pmatrix} 0 & \hat{H}_0 \\ \hat{H}_0^\dagger & 0 \end{pmatrix}. \quad (3)$$

It maps bands of \hat{H}_0 , respectively \hat{H}_0^\dagger , to positive, respectively negative, energies E , Fig. 1, with radius $|E|$. Accordingly, subblock topology is encoded by doubled topology with respect to a doubled gap [1,3].

We define a corresponding doubled Green's function,

$$\mathbb{G}(\omega) = \frac{\mathbb{G}_0(\omega)}{1 - \hat{\mathcal{V}}\mathbb{G}_0(\omega)}, \quad \text{with} \quad \mathbb{G}_0(\omega) = \frac{1}{\omega - \hat{\mathbb{H}}_0}, \quad (4)$$

where $\hat{\mathcal{V}}$ is the doubled impurity potential, $\mathcal{V}(\mathbf{r}_\perp = 0)$, and $\hat{\mathbb{H}} = \hat{\mathbb{H}}_0 + \hat{\mathcal{V}}$. Being Hermitian, the topological edge states correspond to the zeros of the projected doubled Green's function, as before (Supplemental Material IV.2 [29]).

Crucially, we extract the physical meaning of these edge modes by relating doubled Green's function zeros to those of the single Green's function. We parametrize the single Green's functions by $\omega \in \mathbb{R}, \theta \in [0, 2\pi]$,

$$G_0(\omega, \theta) \equiv (\omega e^{i\theta} - \hat{H}_0)^{-1}, \quad (5)$$

and define its complex conjugate, $G_0^\dagger(\omega, -\theta)$, parametrized by $-\theta \in [-2\pi, 0]$, S.I. IV.2 [29]. This is subtle because \mathbb{G}_0 is only defined for $\omega \in \mathbb{R}$, and the zeros of G_0, G_0^\dagger are, in general, complex. However, noting that $\omega^2 = (\omega e^{i\theta})(\omega e^{-i\theta})$ for any $\theta \in [0, 2\pi]$, we may choose θ as a function of ω , defining a path in the complex plane. We can then factor \mathbb{G}_0 (Sec. IV.2 of Ref. [29]) as

$$\mathbb{G}_0 = \begin{pmatrix} 0 & G_0^\dagger \\ G_0 & 0 \end{pmatrix} \left[1 - \omega \begin{pmatrix} 0 & G_0^\dagger \\ G_0 & 0 \end{pmatrix} \begin{pmatrix} -1 & e^{i\theta} \\ e^{-i\theta} & -1 \end{pmatrix} \right]^{-1}. \quad (6)$$

And, we take $\theta(\omega)$ such that our path intersects the zeros, ω_*, θ_* of G_0 . The doubled band gap is thus defined by the radial distance ω between bands as shown in Fig. 1, and “in-gap” zeros of the doubled Hermitian Green's function, \mathbb{G}_0 correspond to in-gap zeros of the single non-Hermitian Green's functions, G_0 .

Non-Hermitian boundary modes.—Projecting the Green's functions to an edge, we come to a main result, the exhaustive

TABLE I. Non-Hermitian boundary modes. Correspondences of in-gap single vs doubled Green’s function zeros (sGF vs dGF) by Eq. (6), see text. Doubled Green’s functions defined with respect to specified gap condition (yes or no indicates presence or absence of zeros). Cases I, II exhibit topological edge modes, those in case III are not topological. Case IV is topologically equivalent to the Hermitian gapless phase.

Case	sGF	dGF	Gap	Manifestation
I	\mathbb{R}	Yes	Any	Traditional bulk boundary
II	$\mathbb{C} - \mathbb{R}$	Yes	Any	Anomalous skin effect
III	Singular	Yes	Point	Trivial skin effect
IV	N/A	No	Point	Gapless Hermitian

determination of boundary modes in non-Hermitian systems, Table I.

First, in the presence of a line gap [Fig. 1(a)], if the projected doubled Green’s function, $\mathbb{G}_0(\omega, \mathbf{k}_{\parallel}, \mathbf{r}_{\perp} = 0)$, has in-gap zeros, we distinguish two topological cases. The projected single Green’s function, $G_0(\omega, \mathbf{k}_{\parallel}, \mathbf{r}_{\perp} = 0)$, either has zeros on (I) or has zeros off (II) the real axis. Case I corresponds to traditional bulk-boundary correspondence—a topologically nontrivial phase hosts edge modes reflecting the bulk topological degeneracy. Case II we refer to as the anomalous skin effect—a topologically nontrivial phase hosts edge modes with complex conjugate energies, a growing and a decaying mode. Since line gap band topology is defined by the doubled Hamiltonian, cases I and II are not topologically distinct and generalize the notion of bulk-boundary correspondence.

Second, consider a single band point gap [Fig. 1(b)]. Edges cut the band and project along corresponding momenta, with two possible outcomes. The point gap is either preserved, or the bands are “flattened”—made contractible to a point—and the point gap topology trivialized. By contrast, the doubled Green’s function topology is defined over the (real) doubled gap before projection [Fig. 1(b)] in both cases. If the point gap survives, a nontrivial topology exhibits corresponding boundary modes by Eq. (6), case I, II. Alternatively, if bands are flattened, the projected spectrum is gapless and the single projected Green’s function is singular. Hence, a bulk point gap invariant does not have corresponding topological edge modes. Instead, we observe a trivial skin effect (case III)—topologically trivial localization of bulk modes at the edge. Heuristically, if an edge destroys the entire bulk topology, it must carry all bulk topological information and hence localize all bulk modes, see also Sec. V.1 of Ref. [29].

Third, consider a topologically trivial line gap topology, an absence of in-gap zeros for the doubled Green’s function. Bands in the complex plane generically form closed loops and thus, also have point gaps, e.g., band centers in Fig. 1(a). The point gap topology is always trivial with respect to the line gap. However, if the point gap

invariant is intrinsically nontrivial and an edge flattens the bands, a trivial skin effect (III) is generated as before. Skin modes are not topological and have energies away from the line gap, lying in the bands, but can be detected by computing the double Green’s function of a single band with respect to its center. Since a band may have both a point gap and line gap invariant, the trivial skin effect may coexist with topological edge-localized modes (I,II).

Finally, consider a band gap such as in Fig. 1(c). Here the doubled Green’s function is directly sensitive to both the band and point gap topology, and the zero crossings are, by definition, separated in energy [Fig. 1(c)]. If the point gap is trivialized, we observe a trivial skin effect, otherwise, we see topological edge modes corresponding to the point gap topology. On top of these modes, the topological edge modes corresponding to the band gap topology can be detected via the same correspondence in Eq. (6), and Table I holds, as above.

The role of symmetry.—Since cases I and II are not topologically distinct, Eq. (6) provides a purely topological generalization of bulk-boundary correspondence protected by the existence of a gap, see Supplemental Material IV.2 [29]. And, traditional bulk-boundary correspondence is a symmetry protected case of the anomalous skin effect [18]. In fact, the spectrum can be continuously rotated in Fig. 1(c), tuning between cases I and II. Furthermore, while a point gap does not protect bulk-boundary correspondence, bulk vs edge symmetries determine the presence of trivial skin modes. This implies a direct classification of non-Hermitian SPTs by their edge modes.

Distinguishing topological invariants.—Characterizing system edge modes, the formalism makes it possible to probe non-Hermitian band topology directly. For example, consider \mathbb{Z} and \mathbb{Z}_2 line gap topological invariants. The edge dispersion parity under time-reversal symmetry (TRS) immediately distinguishes them. This distinction is critical in non-Hermitian systems, where topological invariants depend on gap conditions. In fact, in the example below, we identify a purely non-Hermitian topological phase transition, where line gap separated bands are tuned to a point gap, without altering Hamiltonian symmetries, Fig. 3.

Examples.—We illustrate our universal framework in the context of the non-Hermitian Chern insulator. Our formalism also works for edges of arbitrary codimensions, see also Ref. [27], and for the well-studied non-Hermitian Su-Schrieffer-Heeger (SSH) model, in which we retrieve and clarify the transitions reported in previous works; see Supplemental Material VII.1 [29]. We consider the Hamiltonian

$$\mathcal{H} = \boldsymbol{\xi}(\mathbf{k})\boldsymbol{\sigma} + i\mathbf{h}\boldsymbol{\sigma}, \quad (7)$$

where $\boldsymbol{\sigma} = (\sigma_x, \sigma_y, \sigma_z)$, $\mathbf{h} = (h_x, h_y, h_z)$ indicates the strength of the non-Hermitian field, and $\boldsymbol{\xi}(\mathbf{k}) = (\cos k_x + \cos k_y - m, -\sin k_x, \sin k_y)$. We use the methods in Ref. [27] to

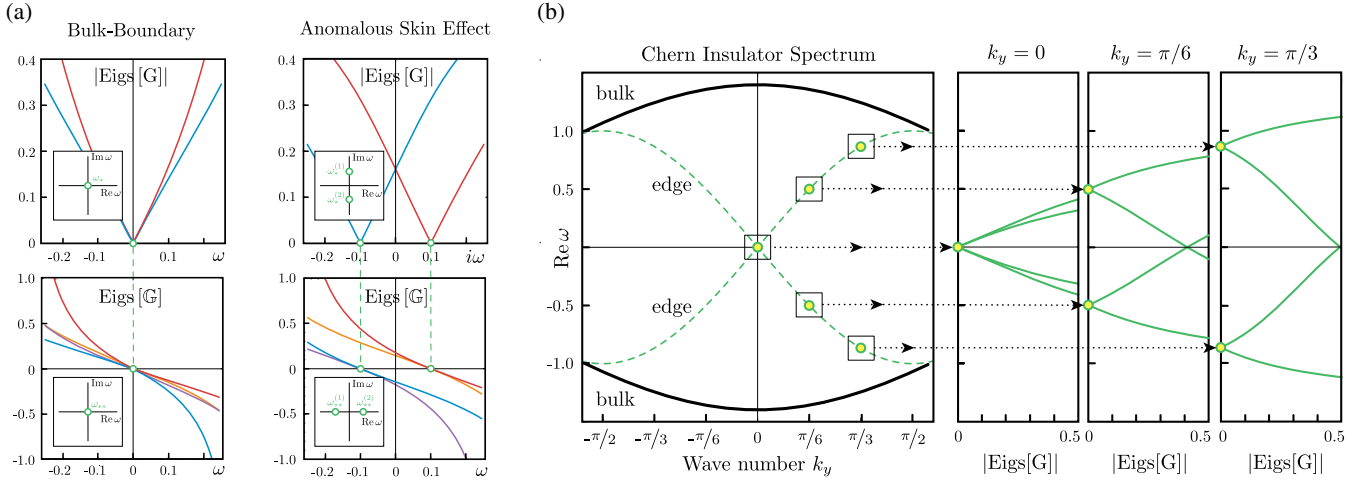


FIG. 2. Non-Hermitian Chern insulator boundary modes. Formalism applied to non-Hermitian Chern insulator, characterizing boundary modes. (a) Top (bottom) row corresponds to single (doubled) Green’s function. System exhibits topological boundary modes: Case I, left column, e.g., $m = 0.4$, $k_y = 0$, $h_x = h_y = 0.1$, $h_z = 0$, and case II, right column, e.g., $m = 0.4$, $k_y = 0$, $h_x = h_y = 0$, $h_z = 0.1$. (red and blue indicate eigenvalue branches) (b) Edge state dispersion ($h_z = 0$, $m = 0.6$, edge along the \hat{y} axis). For every in-plane momentum \mathbf{k}_{\parallel} , each k_y above, we solve for boundary mode energy, defining a dispersion relation.

compute the single and doubled Green’s functions zeros for this model, see Sec. VI.1 of Ref. [29].

In general, the dispersion relation can be read off from the Green’s function zeros. Here, projecting the Hamiltonian to the edge $\hat{x} = 0$, reduces it to the non-Hermitian SSH model, $\xi = [m - \cos(k_y), 0, \sin(k_y)]$. Hence, the edge dispersion is simply given by $\pm[\sin(k_y) + ih_z]$ (Supplemental Material VI.1 [29]) and is real for $h_z = 0$ by a combination of transposition and chiral symmetry [2,14], see Supplemental Material VII [29]. Therefore, we observe a generalized bulk-boundary correspondence, case I for $h_z = 0$ and case II for $h_z \neq 0$, see Fig. 2.

We compute the Chern number via Green’s function zeros, see Supplemental Material VI.3 [29]. If the line gap is well defined, counting single Green’s function zeros

suffices; two (no) zeros between bands imply $\mathcal{C}_1 = \pm 1$ (0), see Fig. 3. The dispersion is odd under TRS [Fig. 2(b)], consistent with a \mathbb{Z} invariant. And, the topological transition between phases is marked by a gapless region, where, as seen by Ref. [14], the Bloch Chern number is not defined, $m_* \pm |h|$ (with $m_* = 2$ marking the Hermitian topological transition). The bands are “inseparable” [5] in the complex plane. This regime is characterized by a point gap invariant.

We examine the topology (vorticity) of the single hybridized band via the doubled Green’s function [see Fig. 1(b)]. Applying the same zero counting argument as above, we see a new uniquely non-Hermitian transition, Fig. 3. For $h_y = h_z = 0$, the Hermitian $m_* = 2$ phase transition is slightly modified. However, when $h_y \neq 0$ or

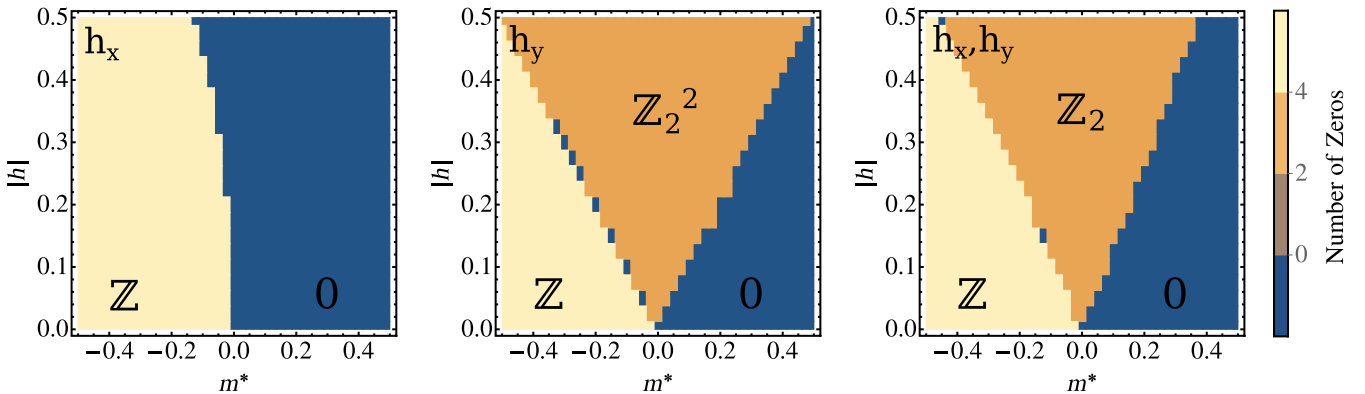


FIG. 3. Non-Hermitian Chern insulator phase diagram.—Phases of non-Hermitian Chern insulator. Nonzero components of non-Hermitian field \mathbf{h} and mass $m^* = 2 - m$ are indicated in figure panels. Transition between 4 and 2 zeros signals line to point gap transition, topological invariants labeled, see Sec. VI.2 [29]. Components of \mathbf{h} chosen to be anisotropic. Shown are representative cases, i.e., h_x, h_y is the same as h_x, h_z (see others in Supplemental Material VI.3 [29]).

$h_z \neq 0$, we see two zeros appear instead of four. We also notice that the doubled dispersion relation in this regime becomes time-reversal symmetric, indicating the bands are indexed by a \mathbb{Z}_2 invariant instead of a \mathbb{Z} invariant, see Supplemental Material VI.2 [29].

This transition is thoroughly understood via all relevant symmetries in Supplemental Material VI.2 [29]. We focus on the case of generic \mathbf{h} , which has a \mathbb{Z} line gap invariant and a \mathbb{Z}_2 point gap invariant. As we increase $|\mathbf{h}|$, the line gap [Fig. 1(a)] closes and forms a point gap [Fig. 1(b)]. While existing methods were unable to provide a direct computation of the topological invariant in this regime [14], our formalism, counting zeros, is sensitive to these transitions, see Fig. 3. In fact, comparing our classification when only $h_y \neq 0$ in the point gap regime to previous work on the non-Hermitian skin effect [2,14], we find trivial skin modes emerge for the same conditions as predicted by the edge-induced trivialization of point gap topology.

Discussion and conclusion.—We presented a universal framework to determine boundary modes in non-Hermitian systems with two major outcomes, see Table I. The first is a generalization of bulk-boundary correspondence to non-Hermitian systems in the presence of a gap. We distinguish two types of topological edge modes, those obeying traditional bulk-boundary correspondence (I) and the anomalous skin effect (II) and demonstrate case I to be a symmetry constraint on the spectrum. This is accomplished via a complete characterization of topological edge modes and their dispersion relations, allowing us to distinguish different topological bulk invariants.

Moreover, the framework detects a uniquely non-Hermitian phase transition under the closing of a line gap [Fig. 1(a)] into a point gap [Fig. 1(b)]. As presented in Table I, nontrivial point gap topology does not guarantee bulk-boundary correspondence, but the skin effect directly stems from its presence and subsequent trivialization due to an edge (case III). And, we detect topological edge modes reflecting a bulk point gap in the latter case (I,II). Thus, our framework makes novel non-Hermitian phase transitions physically accessible and suggests the extended SPT classification [1,3] is relevant beyond fine-tuning. We illustrated this by computing the non-Hermitian Chern insulator phase diagram, Fig. 3, for a gapless parameter regime previously inaccessible [14]. Finally, we remark that our universal formulation in terms of Green's functions allows for the incorporation of interactions in a natural manner, analogously to the Hermitian counterparts [62], making our framework also valuable for this active line of research.

The authors specially thank Jong Yeon Lee for his suggestion to inspect doubled Hamiltonian boundary modes and helpful discussions on the physical significance of edge modes in the presence of a point gap. We also thank Hengyun Zhou for insights on the classification scheme in Ref. [1]. We cordially thank Ashvin Vishwanath, Joaquin Rodriguez Nieva, and Ching Hua

Lee for valuable discussions. A. J. K. was supported by the Swiss National Science Foundation, Grant No. P2ELP2_175278. R.-J. S. appreciatively acknowledges funding via Ashvin Vishwanath.

D. S. B. and R.-J. S. developed the framework, performed calculations, and wrote the manuscript. A. J. K. contributed to the initial numerics and figures.

-
- [1] H. Zhou and J. Y. Lee, *Phys. Rev. B* **99**, 235112 (2019).
 - [2] K. Kawabata, K. Shiozaki, and M. Ueda, *Phys. Rev. B* **98**, 165148 (2018).
 - [3] K. Kawabata, K. Shiozaki, M. Ueda, and M. Sato, *Phys. Rev. X* **9**, 041015 (2019).
 - [4] D. Leykam, K. Y. Bliokh, C. Huang, Y. D. Chong, and F. Nori, *Phys. Rev. Lett.* **118**, 040401 (2017).
 - [5] H. Shen, B. Zhen, and L. Fu, *Phys. Rev. Lett.* **120**, 146402 (2018).
 - [6] S. Yao and Z. Wang, *Phys. Rev. Lett.* **121**, 086803 (2018).
 - [7] K. Esaki, M. Sato, K. Hasebe, and M. Kohmoto, *Phys. Rev. B* **84**, 205128 (2011).
 - [8] Z. Gong, Y. Ashida, K. Kawabata, K. Takasan, S. Higashikawa, and M. Ueda, *Phys. Rev. X* **8**, 031079 (2018).
 - [9] R. El-Ganainy, K. G. Makris, M. Khajavikhan, Z. H. Musslimani, S. Rotter, and D. N. Christodoulides, *Nat. Phys.* **14**, 11 (2018).
 - [10] A. Guo, G. J. Salamo, D. Duchesne, R. Morandotti, M. Volatier-Ravat, V. Aimez, G. A. Siviloglou, and D. N. Christodoulides, *Phys. Rev. Lett.* **103**, 093902 (2009).
 - [11] C. E. Rüter, K. G. Makris, R. El-Ganainy, D. N. Christodoulides, M. Segev, and D. Kip, *Nat. Phys.* **6**, 192 (2010).
 - [12] J. M. Zeuner, M. C. Rechtsman, Y. Plotnik, Y. Lumer, S. Nolte, M. S. Rudner, M. Segev, and A. Szameit, *Phys. Rev. Lett.* **115**, 040402 (2015).
 - [13] H. Zhou, C. Peng, Y. Yoon, C. W. Hsu, K. A. Nelson, L. Fu, J. D. Joannopoulos, M. Soljačić, and B. Zhen, *Science* **359**, 1009 (2018).
 - [14] S. Yao, F. Song, and Z. Wang, *Phys. Rev. Lett.* **121**, 136802 (2018).
 - [15] V. M. Martínez Alvarez, J. E. Barrios Vargas, M. Berdakin, and L. E. F. Foa Torres, *Eur. Phys. J. Spec. Top.* **227**, 1295 (2018).
 - [16] C. H. Lee and R. Thomale, *Phys. Rev. B* **99**, 201103 (2019).
 - [17] F. K. Kunst, E. Edvardsson, J. C. Budich, and E. J. Bergholtz, *Phys. Rev. Lett.* **121**, 026808 (2018).
 - [18] L. Jin and Z. Song, *Phys. Rev. B* **99**, 081103(R) (2019).
 - [19] A. Kitaev, *AIP Conf. Proc.* **1134**, 22 (2009).
 - [20] L. Fu, *Phys. Rev. Lett.* **106**, 106802 (2011).
 - [21] R.-J. Slager, A. Mesaros, V. Juričić, and J. Zaanen, *Nat. Phys.* **9**, 98 (2013).
 - [22] J. Kruthoff, J. de Boer, J. van Wezel, C. L. Kane, and R.-J. Slager, *Phys. Rev. X* **7**, 041069 (2017).
 - [23] H. C. Po, A. Vishwanath, and H. Watanabe, *Nat. Commun.* **8**, 50 (2017).
 - [24] B. Bradlyn, L. Elcoro, J. Cano, M. G. Vergniory, Z. Wang, C. Felser, M. I. Aroyo, and B. A. Bernevig, *Nature (London)* **547**, 298 (2017).
 - [25] K. Shiozaki and M. Sato, *Phys. Rev. B* **90**, 165114 (2014).

- [26] J. Höller and A. Alexandradinata, *Phys. Rev. B* **98**, 024310 (2018).
- [27] R.-J. Slager, L. Rademaker, J. Zaanen, and L. Balents, *Phys. Rev. B* **92**, 085126 (2015).
- [28] J.-W. Rhim, J. H. Bardarson, and R.-J. Slager, *Phys. Rev. B* **97**, 115143 (2018).
- [29] See Supplemental Material at <http://link.aps.org/supplemental/10.1103/PhysRevLett.124.056802>. In this Supplemental Material the presented framework is further discussed and illustrated with a variety of models. This relates our work to earlier specific observations and general topological notions, connecting to Refs. [30–59].
- [30] Z. Wang and S.-C. Zhang, *Phys. Rev. X* **2**, 031008 (2012).
- [31] T. Fukui, T. Fujiwara, and Y. Hatsugai, *J. Phys. Soc. Jpn.* **77**, 123705 (2008).
- [32] R. M. Kaufmann, D. Li, and B. Wehefritz-Kaufmann, *Rev. Math. Phys.* **28**, 1630003 (2016),
- [33] K. Kawabata, S. Higashikawa, Z. Gong, Y. Ashida, and M. Ueda, *Nat. Commun.* **10**, 297 (2019).
- [34] H.-G. Zirnstein, G. Refael, and B. Rosenow, [arXiv:1901.11241](https://arxiv.org/abs/1901.11241).
- [35] A. M. Essin and V. Gurarie, *Phys. Rev. B* **84**, 125132 (2011).
- [36] Y. Hatsugai, *Phys. Rev. Lett.* **71**, 3697 (1993).
- [37] A. Mesaros, R.-J. Slager, J. Zaanen, and V. Juričić, *Nucl. Phys.* **B867**, 977 (2013).
- [38] S. Ryu, A. P. Schnyder, A. Furusaki, and A. W. Ludwig, *New J. Phys.* **12**, 065010 (2010).
- [39] R.-J. Slager, V. Juričić, and B. Roy, *Phys. Rev. B* **96**, 201401 (R) (2017).
- [40] R.-J. Slager, V. Juričić, V. Lahtinen, and J. Zaanen, *Phys. Rev. B* **93**, 245406 (2016).
- [41] L. Herviö, J. H. Bardarson, and N. Regnault, *Phys. Rev. A* **99**, 052118 (2019).
- [42] Y. Xiong, *J. Phys. Commun.* **2**, 035043 (2018).
- [43] J. Carlström, M. Stalhammar, J. C. Budich, and E. J. Bergholtz, *Phys. Rev. B* **99**, 161115(R) (2019).
- [44] C. H. Lee, G. Li, Y. Liu, T. Tai, R. Thomale, and X. Zhang, [arXiv:1812.02011](https://arxiv.org/abs/1812.02011).
- [45] A. Mostafazadeh, *J. Math. Phys. (N.Y.)* **43**, 205 (2002).
- [46] C. M. Bender and S. Boettcher, *Phys. Rev. Lett.* **80**, 5243 (1998).
- [47] J. Feinberg and A. Zee, *Phys. Rev. E* **59**, 6433 (1999).
- [48] F. K. Kunst and V. Dwivedi, *Phys. Rev. B* **99**, 245116 (2019).
- [49] V. M. Martinez Alvarez, J. E. Barrios Vargas, and L. E. F. Foa Torres, *Phys. Rev. B* **97**, 121401(R) (2018).
- [50] D. Porras and S. Fernández-Lorenzo, *Phys. Rev. Lett.* **122**, 143901 (2019).
- [51] Y. Chen and H. Zhai, *Phys. Rev. B* **98**, 245130 (2018).
- [52] M. R. Hirsbrunner, T. M. Philip, and M. J. Gilbert, *Phys. Rev. B* **100**, 081104 (2019).
- [53] V. Juričić, A. Mesaros, R.-J. Slager, and J. Zaanen, *Phys. Rev. Lett.* **108**, 106403 (2012).
- [54] A. Bouhon, A. M. Black-Schaffer, and R.-J. Slager, *Phys. Rev. B* **100**, 195135 (2019).
- [55] R.-J. Slager, *J. Phys. Chem. Solids* **128**, 24 (2019).
- [56] R.-J. Slager, A. Mesaros, V. Juričić, and J. Zaanen, *Phys. Rev. B* **90**, 241403(R) (2014).
- [57] A. J. Heeger, S. Kivelson, J. R. Schrieffer, and W. P. Su, *Rev. Mod. Phys.* **60**, 781 (1988).
- [58] S. Lieu, *Phys. Rev. B* **97**, 045106 (2018).
- [59] C. Yin, H. Jiang, L. Li, R. Lü, and S. Chen, *Phys. Rev. A* **97**, 052115 (2018).
- [60] B. A. Bernevig and T. L. Hughes, *Topological Insulators and Topological Superconductors* (Princeton University Press, Princeton, 2013).
- [61] R. Roy and F. Harper, *Phys. Rev. B* **96**, 155118 (2017).
- [62] S. Raghu, X.-L. Qi, C. Honerkamp, and S.-C. Zhang, *Phys. Rev. Lett.* **100**, 156401 (2008).